JACS
JOURNAL OF THE AMERICAN CHEMICAL SOCIETY
pubs.acs.org/JACS

Article

Electrochemical CO_2 Reduction in the Presence of SO_2 Impurities on a Nitrogen-Doped Carbon Electrocatalyst

Shilong Fu, Bowen Sha, Asvin Sajeev, Ming Li, Thijs J. H. Vlugt, Othonas A. Moultos, Wiebren de Jong, and Ruud Kortlever*

Cite This: https://doi.org/10.1021/jacs.5c11790

Read Online

ACCESS | Metrics & More | Article Recommendations | Supporting Information

ABSTRACT: Electrochemical CO_2 reduction to CO offers a sustainable route for converting CO_2 into value-added chemicals and fuels. However, CO_2 streams derived from industrial sources often contain SO_2 impurities that severely poison conventional metal-based catalysts. Here, we report a nitrogen-doped carbon catalyst that exhibits pronounced tolerance and stability for CO_2-to-CO conversion in the presence of SO_2 (100−10,000 ppm). The catalyst maintains over 90% Faradaic efficiency toward CO during 8 h of electrolysis at −1.0 V vs RHE with 100 ppm of SO_2, whereas Ag foil electrodes undergo rapid deactivation. Density functional theory calculations combined with surface analyses indicate that weak SO_2 adsorption and the absence of stable sulfur accumulation on nitrogen-doped carbon strengthen its resistance to impurity-induced deactivation, in contrast to Ag catalysts that form Ag_2S. Gas-fed tests in a membrane electrode assembly (MEA) electrolyzer further confirm that nitrogen-doped carbon sustains high CO selectivity at elevated current densities, while Ag nanoparticles suffer irreversible sulfur poisoning. These results demonstrate that nitrogen-doped carbon is intrinsically resistant to SO_2-induced deactivation and highlight its potential as a robust catalyst for CO_2 electroreduction under impurity-containing conditions.

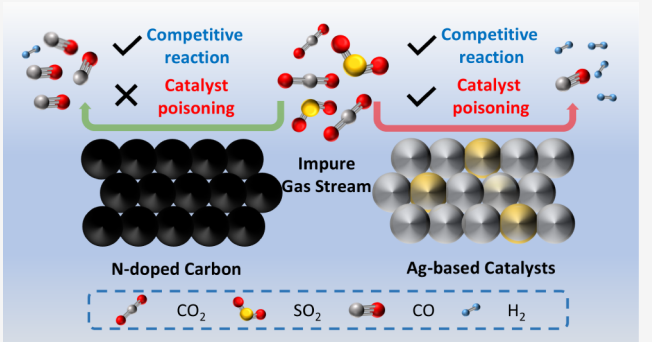

INTRODUCTION

Coupling clean and renewable energy sources with the electrochemical CO_2 reduction reaction (CO_2RR) is a promising approach to convert waste CO_2 to value-added chemicals and fuels and to store intermittent energy in chemical bonds.[1,2] Depending on the electrocatalyst and reaction conditions, CO_2 can be selectively reduced to various products, including CO, formate, CH_4, C_2H_4 and oxygenated hydrocarbons.[3,4] Among these, CO stands out as an attractive product due to its relatively high selectivity and potential for large-scale applications.[5]

Despite significant progress, almost all high-performance electrocatalysts for CO production have been tested under ideal conditions using high-purity CO_2 gas (≥99.99%) to avoid contaminations.[6−9] However, industrial CO_2-rich streams, such as flue gases from power plants and metallurgical industry, typically contain gaseous impurities such as sulfur oxides (SO_x) and nitrogen oxides (NO_x)[10−12] that can detrimentally impact CO_2RR performance. In particular, SO_2 is one of the most prevalent contaminants in industrial CO_2 sources, typically present in concentrations ranging from approximately 100 to 10,000 ppm depending on the emission source and purification level.[13] Recent studies on metallic catalysts (e.g., copper, silver, and tin) have shown that these impurities can trigger side reactions, induce catalyst surface reconfiguration, and cause deactivation, resulting in reduced faradaic efficiency and altered product selectivity (Table S1).[14−17]

However, existing studies have generally examined only one or two impurity concentrations at a fixed potential or current density, providing limited insight into the broader impact of these contaminants. Systematic investigations across various impurity concentrations and operating conditions are needed to develop impurity-tolerant catalysts.[18] Although impurity removal through scrubbing and absorption is possible, several techno-economic analyses reveal that the purification processes significantly increase the cost for CO_2 utilization.[19,20] In this sense, developing stable electrocatalysts that can operate efficiently with impure CO_2 feedstocks is crucial for the sustainable scale-up of CO_2RR to CO.

Nitrogen-doped (N-doped) carbon materials have emerged as highly efficient and cost-effective electrocatalysts for the electrochemical reduction of CO_2 to CO, providing a promising alternative to traditional metal-based catalysts.[21−23] In previous

Received: July 10, 2025
Revised: December 27, 2025
Accepted: December 30, 2025

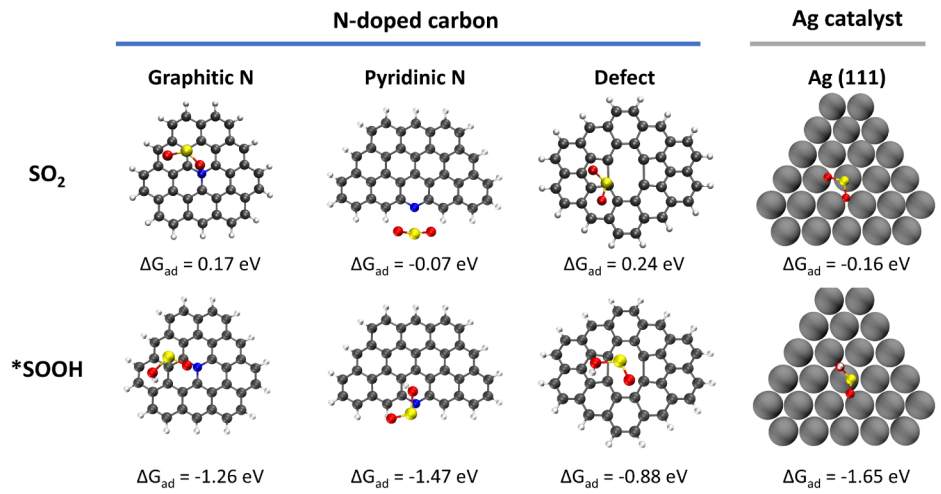

Figure 1. SO_2 and *SOOH adsorption on nitrogen-doped carbon and silver surfaces. A comparison of SO_2 and *SOOH adsorption modes and ΔG_{ad} adsorption energies on three potential active sites of N-doped carbon catalysts, namely graphitic nitrogen, pyridinic nitrogen, and carbon defects, and on the Ag(111) surface.

studies, we developed a series of biomass-derived N-doped carbon catalysts and revealed the correlation between the physicochemical properties of N-doped biochar catalysts and their CO_2RR performance.[24,25] By systematically altering factors such as the type of activating agent, carbonization temperature, and nitrogen doping level, a tailored N-doped biochar catalyst was synthesized, achieving over 90% faradaic efficiency for CO production.

A key advantage of carbon-based catalysts is their inherent resistance to acidic and basic environments,[26] which suggests that N-doped carbon materials can exhibit significant stability for CO_2RR even when exposed to common gaseous impurities found in industrial CO_2 streams. However, despite this potential, there is currently no comprehensive understanding of how these contaminants affect the CO_2RR activity and stability of N-doped carbon catalysts. Further investigation is needed to explore the influence of various impurities on their performance, which could provide critical insights for designing robust, impurity-resistant electrocatalysts for practical applications.

In this study, we assess the impact of SO_2 impurities on the electrocatalytic performance of an activated nitrogen-doped biochar (ANBC) catalyst for electrochemical CO_2 reduction to CO. For comparison, a silver foil (Ag foil) electrode, one of the most widely used electrocatalyst for CO_2 reduction to CO, was used as a reference. However, given the distinct physical forms of the catalysts (powder versus foil), it is important to note that the comparisons between ANBC and Ag foil are interpreted qualitatively, focusing on differences in electrocatalytic behavior rather than a direct quantitative performance comparison.

Density functional theory calculations reveal that N-doped carbon displays lower adsorption energies for SO_2 and *SOOH than silver, highlighting their inherent potential for resisting SO_2 impurities. Experimental results further demonstrate that the N-doped carbon catalyst displayed a stronger tolerance to SO_2 impurities, maintaining higher faradaic efficiency and stability for CO production, no significant changes in surface structure or composition were observed on the ANBC catalyst. However, the Ag foil is highly sensitive to SO_2 contaminations, exhibiting a pronounced decline in CO_2RR performance due to surface poisoning and the competing SO_2 reduction reaction.

To further validate the practical applicability of ANBC under gas-fed conditions, high current density electrolysis tests were conducted using a membrane electrode assembly (MEA) reactor. Under operation at 100 mA/cm^2, the ANBC electrode maintained high CO selectivity and structural integrity, whereas Ag nanoparticle electrodes suffered rapid deactivation due to the progressive formation of Ag_2S. These MEA results are consistent with the findings from H-cell measurements, confirming the exceptional SO_2 tolerance, stability, and robustness of ANBC at technologically relevant current densities.

These results demonstrate that N-doped carbon catalysts exhibit greater resilience to SO_2 impurities compared to Ag-based electrodes, maintaining stable CO_2 reduction performance under challenging conditions. This study provides valuable insights into the tolerance of nonmetallic catalysts to industrial contaminants, highlighting their potential for practical applications in CO_2 conversion processes using impure feedstocks.

RESULTS AND DISCUSSION

Evaluating the Adsorption Energies of SO_2 Impurities via Density Functional Theory Calculations

Density functional theory (DFT) calculations were performed to evaluate the Gibbs free energy of adsorption (ΔG_{ad}) for SO_2 impurities and the critical intermediate *SOOH on both N-doped carbon and silver electrode surfaces (computational methods included in the Supporting Information). Given the ongoing debate regarding the active sites in N-doped carbon materials, where pyridinic nitrogen, graphitic nitrogen, and carbon defects have all been proposed as active sites, we comprehensively evaluated the adsorption free energies of SO_2 and *SOOH on these three sites. For the silver electrode, the predominant (111) facet was considered.

The adsorption energy results demonstrate that all three potential active sites on N-doped carbon materials exhibit weaker adsorption for both SO_2 and *SOOH compared to the Ag (111) surface (Figure 1). This indicates a lower binding energy between the N-doped carbon materials and these sulfur-containing species relative to the silver electrode. The stronger adsorption affinity of the silver surface directly correlates with its higher susceptibility to SO_2 poisoning. Consequently, N-doped carbon materials demonstrate superior tolerance to SO_2

https://doi.org/10.1021/jacs.5c11790
J. Am. Chem. Soc. XXXX, XXX, XXX−XXX

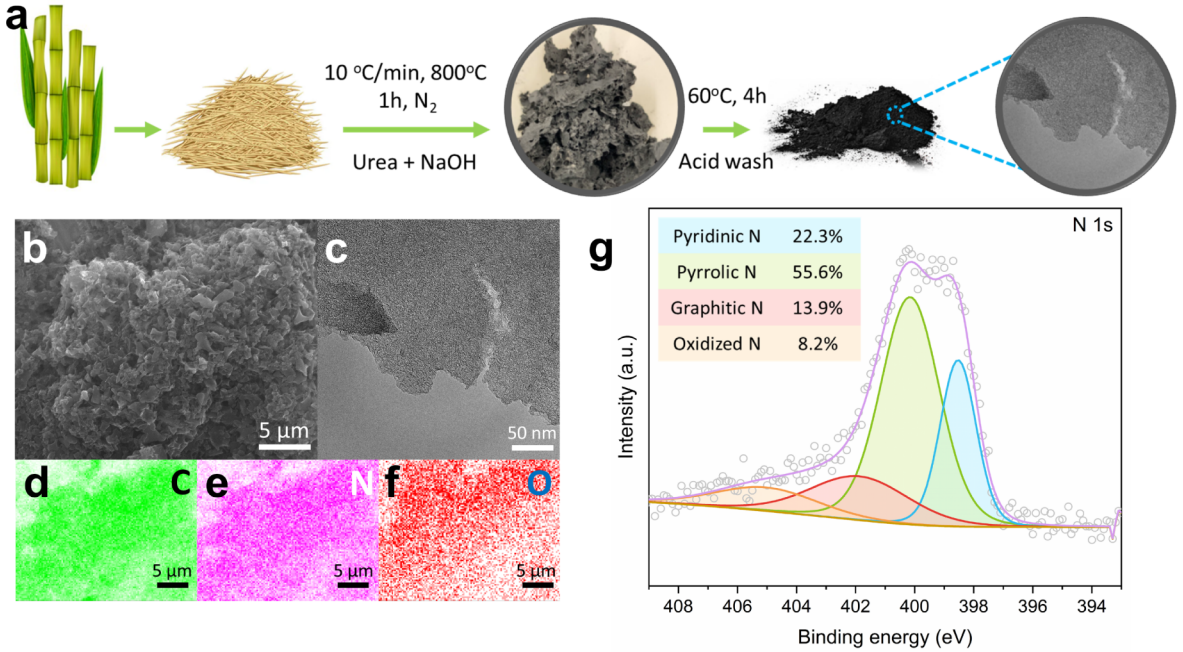

Figure 2. Synthesis and characterization of activated nitrogen-doped biochar. (a) A schematic illustration of the synthesis method of the ANBC catalyst; (b) SEM image; (c) TEM image; (d–f) EDX mapping images; and (g) high-resolution XPS N 1s spectrum of the synthesized ANBC.

poisoning compared to silver electrodes. More specifically, the adsorption of SO_2 and *SOOH on graphitic N sites and carbon defects is weaker than on edge-located pyridinic N sites. This difference arises from the distinct electronic properties of the nitrogen functionalities: graphitic N carries a partial positive charge, while pyridinic N bears a partial negative charge. Consequently, their adsorption modes for SO_2 diverge, graphitic N preferentially interacts with the negatively charged oxygen atom, whereas pyridinic N adsorbs via the positively charged sulfur atom. It is important to note that the partial charges of nitrogen and SO_2 atoms only describe their preferred adsorption orientation, rather than the magnitude of electrostatic binding. The overall SO_2 adsorption is not purely governed by electrostatics but by a combination of electronic structure modulation, orbital overlap, and adsorption configuration effects. In summary, all three potential active sites in N-doped carbon catalysts exhibit lower adsorption energies for SO_2 and *SOOH than the Ag(111) surface, highlighting their inherent potential for resisting SO_2 impurity poisoning.

Building upon the wave functions obtained from DFT simulations, Independent Gradient Model based on Hirshfeld partition (IGMH) analyses were performed using the Multiwfn software.[27−29] On the IGMH isosurfaces, green regions signify weak van der Waals interactions between species, while blue regions indicate stronger attractive interactions (e.g., ionic bonding, hydrogen bonding). The IGMH analyses confirm significantly weaker adsorption of both SO_2 and *SOOH on all three potential active sites of N-doped carbon catalysts compared to silver (Figure S1). Furthermore, the analysis reveals distinct interaction mechanisms. For instance, while electrostatic interactions contribute to SO_2 adsorption at pyridinic N sites, adsorption at graphitic N sites and carbon defects is primarily driven by van der Waals forces. In contrast, adsorption on the silver surface involves codominant electrostatic and van der Waals interactions, thus demonstrating a stronger inherent affinity for sulfur-containing species than the carbon materials.

Further electronic structure analysis was performed using the Multiwfn package to compute the density of states (DOS), projected density of states (PDOS), and overlap population density of states (OPDOS) based on Mulliken population analysis.[30,31] These calculations elucidate orbital interactions between SO_2 and the surfaces of N-doped carbon materials and the silver electrode (Figure S2). The DOS profiles depict the distribution of quantum states across energy levels. PDOS decomposes this distribution into fragment contributions, enabling identification of specific atomic/molecular orbital involvement. Crucially, OPDOS analysis identifies quantum states exhibiting positive overlap populations, thereby highlighting energy regions conducive to constructive orbital interactions between fragments. Distinct OPDOS peaks near −13 eV and −9 eV were observed for SO_2 adsorption on all three N-doped active sites and the Ag(111) surface. Notably, silver's abundant d-electrons generate densely packed electronic states across the −8 eV to −5 eV energy range. This d-band broadening significantly extends the energy window for orbital hybridization with SO_2, consequently enhancing orbital interactions on silver relative to N-doped carbon catalysts.

In addition, we compared the adsorption energies of CO_2 and SO_2 on various active sites of N-doped carbon and on the Ag(111) surface. The calculated adsorption energies of CO_2 on graphitic-N, pyridinic-N, carbon defect, and Ag(111) sites were approximately 0.22, 0.26, 0.11, and 0.18 eV, respectively. In contrast, SO_2 exhibited adsorption energies of about 0.17 eV, −0.07 eV, 0.24 eV, and −0.16 eV at the corresponding sites (Figure S3). These results indicate that SO_2 generally shows slightly stronger or comparable adsorption affinity than CO_2 on most sites, implying potential competitive adsorption between SO_2 and CO_2. As the SO_2 concentration increases, SO_2 may increasingly occupy active sites, thereby suppressing CO_2 reduction. It is worth noting, however, that both CO_2 and SO_2 exhibit relatively weak interactions with ANBC, suggesting limited physical adsorption and minimal surface reconstruction. In contrast, Ag displays distinct adsorption behavior: while CO_2

https://doi.org/10.1021/jacs.5c11790
J. Am. Chem. Soc. XXXX, XXX, XXX−XXX

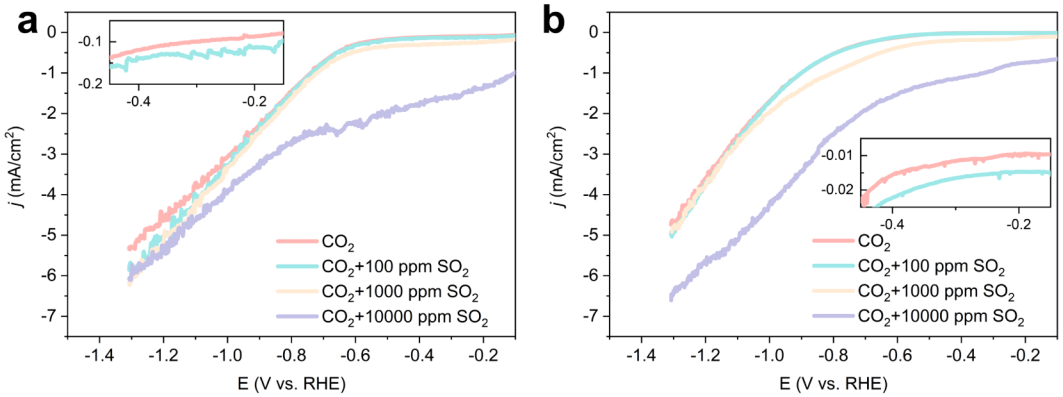

Figure 3. Voltammograms of ANBC and silver with varying SO_2 concentrations. LSV curves of (a) ANBC electrodes and (b) Ag foil electrodes, recorded in a 0.1 M $KHCO_3$ catholyte saturated with CO_2, both without SO_2 and in the presence of varying concentrations of SO_2 impurities.

binds only weakly to the Ag surface, SO_2 and its reduction intermediates interact much more strongly (Figure S4). This stronger binding can lead to gradual surface compositional changes, ultimately causing catalyst poisoning and altering product selectivity.

In summary, N-doped carbon catalysts exhibit weaker adsorption energies for both SO_2 and *SOOH compared to the silver electrode. Interactions between sulfur-containing species and N-doped carbon active sites are predominantly governed by van der Waals forces. Furthermore, orbital interactions between SO_2 molecules and the surface structures of N-doped carbon active sites are significantly weaker than those observed on the silver surface. Collectively, these properties strongly suggest that N-doped carbon materials possess superior tolerance to SO_2 impurity poisoning relative to silver electrodes, positioning them as a promising alternative catalyst material in SO_2-containing environments.

Preparation and Properties of Activated N-Doped Biochar (ANBC)

The synthesis strategy of activated nitrogen-doped biochar (ANBC) is illustrated in Figure 2a (experimental details included in the Supporting Information). This specific strategy was selected since it yields an ANBC catalyst with superior performance in CO_2 electroreduction, as demonstrated in our previous study.[25] The synthesis method was systematically optimized in earlier work by varying the type of activating agent, carbonization temperature, and other key parameters, resulting in a material with tailored physicochemical properties that significantly outperformed other catalysts tested. The optimized conditions produce an ANBC catalyst with enhanced porosity, high surface area, and well-dispersed nitrogen heteroatoms, which are crucial for efficient CO_2RR. Given its outstanding activity, this catalyst was resynthesized and employed in the present study to investigate its selectivity and robustness under more challenging conditions.

The morphology and microstructure of the synthesized ANBC were visualized using scanning electron microscopy equipped with energy-dispersive X-ray spectroscopy (SEM-EDX) and transmission electron microscopy (TEM). SEM image reveals an interconnected, three-dimensional architecture with multiscale channels, contributing to its high surface area and porosity (Figure 2b). The EDX elemental mapping confirms a uniform distribution of nitrogen atoms within the carbon matrix (Figure 2d–f). The TEM image indicates a wrinkled nanosheet structure with abundant pores of ANBC, highlighting its high porosity (Figure 2c).

The crystallographic properties of ANBC were evaluated using X-ray diffraction (XRD) and Raman spectroscopy. The XRD pattern exhibits two broad peaks at approximately $2\theta = 25°$ and 44°, corresponding to the (002) and (100) diffraction planes of graphitic carbon, indicating a predominantly amorphous structure (Figure S5a).[32] The Raman spectrum displays two characteristic peaks at ~1350 cm^{-1} (D band) and ~1590 cm^{-1} (G band) that are indicative of disordered carbon and graphitic domains, respectively (Figure S5b).[33] The intensity ratio of these bands (I_D/I_G = 1.097) suggests a high degree of structural defects and a relatively low graphitization level, aligning well with the amorphous nature revealed by the XRD analysis.

N_2 adsorption–desorption isothermal analysis was executed to further evaluate the specific surface area and porosity of the ANBC catalyst. The sample exhibits a combination of type I and type IV isotherms based on the IUPAC classification (Figure S6a). The steep rise in adsorption at low relative pressures indicates a significant presence of micropores, while the emergence of a subtle hysteresis loop between 0.45 and 0.95 relative pressure suggests the incorporation of mesopores. Additionally, a sharp increase in adsorption near saturation pressure (0.95–1.0) points to the existence of macropores in the structure.[34] The pore size distribution, determined via density functional theory, reveals a pronounced peak around 2 nm and a minor peak near 40 nm (Figure S6b). These features contribute to the ANBC's high specific surface area of 1434.7 m^2/g and a total pore volume of 0.68 cm^3/g, along with a hierarchical pore network comprising approximately 19.7% mesopores. The elemental composition and chemical states were analyzed using X-ray photoelectron spectroscopy (XPS). The survey spectrum indicates distinct peaks at 285.1, 400.1, and 533.3 eV, corresponding to the C 1s, N 1s, and O 1s signals, respectively (Figure S7). The total nitrogen content was quantified to be 3.8 at. %. The high-resolution N 1s spectrum is deconvoluted into four peaks at 398.2, 400.2, 401.9, and 404.9 eV, corresponding to pyridinic N (22.3%), pyrrolic N (55.6%), graphitic N (13.9%), and oxidized N (8.2%) configurations (Figure 2g).[35] These XPS results indicate that pyrrolic and pyridinic nitrogen dominate the nitrogen species in ANBC, which is known to play a crucial role in enhancing CO_2RR activity.[22] Overall, the comprehensive characterization results confirm the successful synthesis of an N-doped biochar catalyst featuring uniform nitrogen incorporation, a high specific surface area, and a well-defined

https://doi.org/10.1021/jacs.5c11790
J. Am. Chem. Soc. XXXX, XXX, XXX–XXX

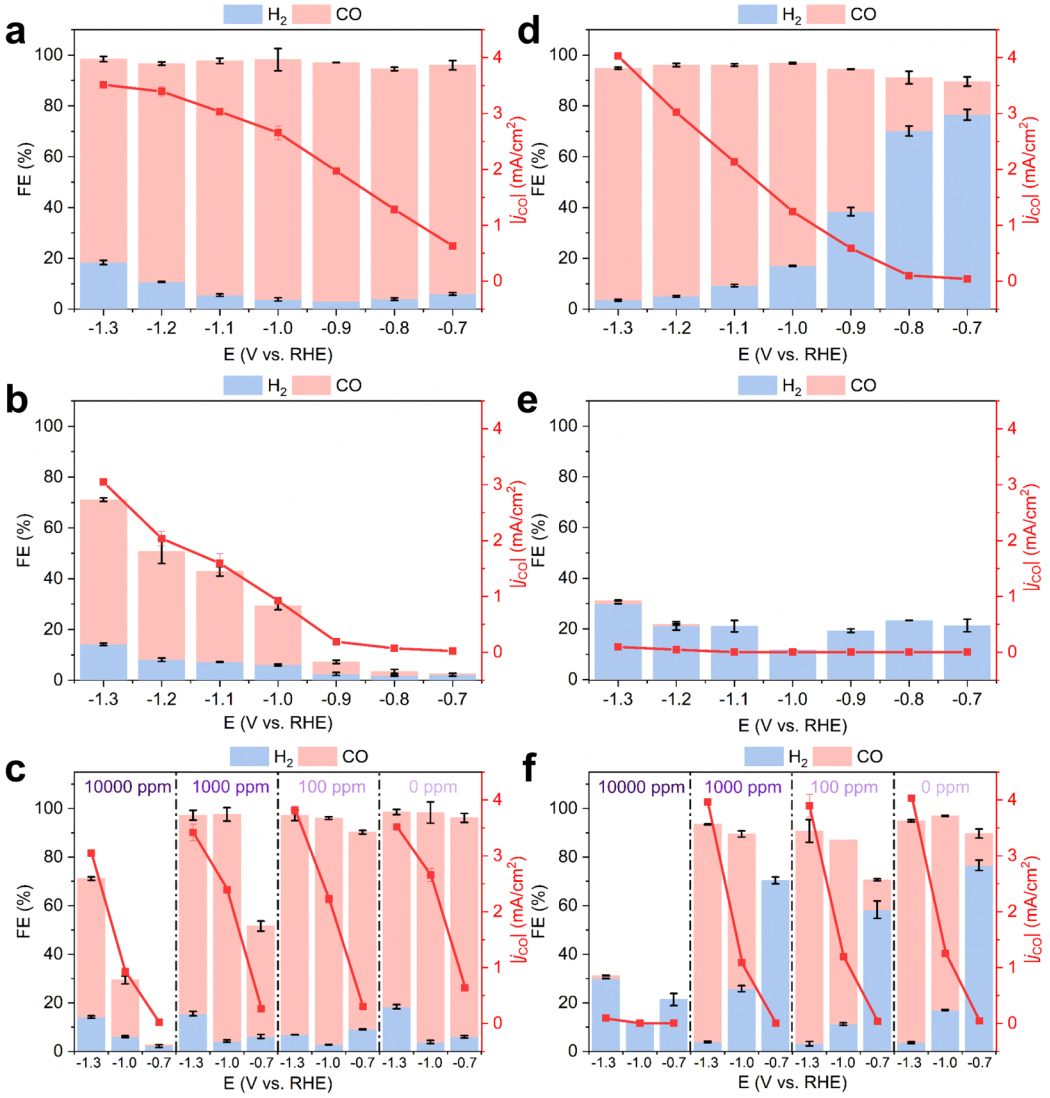

Figure 4. Electrochemical CO_2 reduction performance of ANBC and silver at varying SO_2 concentrations. Faradaic efficiencies and partial current densities for CO production on (a) ANBC and (d) Ag foil electrodes in a CO_2-saturated 0.1 M $KHCO_3$ electrolyte with varying applied potentials, from −0.7 to −1.3 V vs RHE. Faradaic efficiencies and partial current densities for CO production on (b) ANBC and (e) Ag foil electrodes in the presence of 10,000 ppm of SO_2 impurity, from −0.7 to −1.3 V vs RHE. Faradaic efficiencies and partial current densities for CO production on (c) ANBC and (f) Ag foil electrodes with the presence of different concentrations of SO_2 impurities at −0.7, −1.0, and −1.3 V vs RHE.

hierarchical porous structure. These characterization results are consistent with our previous work, demonstrating the reproducibility and reliability of the synthesis method. Collectively, these characteristics indicate that the prepared catalyst is a promising candidate for efficient electrochemical CO_2 reduction to CO, underscoring its potential for practical applications in CO_2 conversion processes.[36−38]

Impact of SO_2 Concentrations and Applied Potentials on the CO_2RR Performance of ANBC and Silver

All electrochemical measurements were performed in a two-compartment compact H-cell (Supporting Information; Figures S8−S9 and Tables S2−S3). Linear sweep voltammetry (LSV) was first conducted for ANBC and Ag foil electrodes in 0.1 M $KHCO_3$ saturated with CO_2 containing different concentrations of SO_2, over a potential window from −0.1 to −1.3 V vs RHE at a scan rate of 5 mV/s. For the ANBC electrode, the LSV curves exhibit a pronounced increase in cathodic current at potentials more negative than approximately −0.6 to −0.7 V vs RHE (Figure 3a). The voltammogram recorded in the presence of 100 ppm of SO_2 closely overlaps with that obtained under pure CO_2, indicating a negligible influence at low SO_2 concentrations. Increasing the SO_2 concentration to 1000 ppm results in a modest enhancement of current density between −0.1 and −0.8 V vs RHE, whereas a substantially larger current response is observed when the SO_2 concentration reaches 10,000 ppm, particularly at less negative potentials. A similar qualitative trend is observed for the Ag foil electrode; however, the current response is markedly more sensitive to the presence of SO_2, especially at higher impurity levels (Figure 3b).

This behavior can be attributed to the intrinsically more favorable electrochemical reduction of SO_2 relative to CO_2. As summarized in Table S4, the standard equilibrium potential for SO_2 reduction is significantly more positive than those of CO_2 reduction and the hydrogen evolution reaction, conferring a clear thermodynamic advantage to SO_2RR.[39] Consistent with prior electrochemical studies, SO_2 reduction has been reported to initiate at potentials in the range of approximately −0.06 to

https://doi.org/10.1021/jacs.5c11790
J. Am. Chem. Soc. XXXX, XXX, XXX−XXX

−0.26 V vs RHE, which are considerably more positive than typical CO_2RR onset potentials.[40] Consequently, at high SO_2 concentrations, SO_2 reduction is readily activated and dominates the cathodic current response. Our density functional theory calculations further support this interpretation, revealing that SO_2 exhibits comparable or stronger adsorption than CO_2 on both ANBC and Ag surfaces, enabling SO_2 to preferentially occupy active sites under elevated concentrations (Figure S3). The combined effects of favorable equilibrium potentials and competitive adsorption explain the pronounced current increase and suppression of CO_2RR observed in the LSV measurements at high SO_2 concentrations (Figure 3). In contrast, at lower SO_2 concentrations, the limited surface coverage of SO_2 results in a much weaker impact, allowing CO_2 reduction to remain the dominant reaction pathway.

We benchmarked the electrochemical performance of the ANBC electrode by performing chronoamperometry measurements in a CO_2 feedstock free of SO_2 impurities (see Figure 4a). CO and H_2 are the main gaseous products detected by the in-line GC and no liquid products were detected with HPLC. The faradaic efficiency toward CO (FE_{CO}) for ANBC is consistently above 80% in a wide potential window from −0.7 V to −1.3 V vs RHE and reaches a maximum of 94.5% FE_{CO} at −1.0 V vs RHE. The partial current density of CO (j_{CO}) gradually increases from −0.63 mA/cm^2 at −0.7 V vs RHE to −3.51 mA/cm^2 at −1.3 V vs RHE. By contrast, the FE_{CO} of the Ag foil electrode increased from 13.1% at −0.7 V vs RHE to 91.4% at −1.3 V vs RHE; however, the j_{CO} of the Ag foil electrode only surpassed that of the ANBC electrode at potentials below −1.2 V vs RHE (Figure 4d).

We further evaluated the CO_2RR performance of the ANBC electrode in the presence of varying concentrations of SO_2 impurities. The concentration of SO_2 in flue gases typically varies from 100 to 10,000 ppm, depending on the chemical composition of fuels and post-treatment strategies.[13] To explore the impact of extreme conditions, we first selected the most challenging scenario, utilizing a gas mixture of CO_2 and 10,000 ppm of SO_2. Under these conditions, the faradaic efficiency of ANBC electrodes toward CO_2RR products significantly declined across the entire potential range (Figure 4b), which is attributed to the preferential reduction of SO_2 over CO_2 (Table S4). Notwithstanding, the FE_{CO} of ANBC increased from only 0.5% at −0.7 V vs RHE to 57% at −1.3 V vs RHE. Moreover, the j_{CO} increased to −3.04 mA/cm^2 at −1.3 V vs RHE, only slightly lower than that observed with pure CO_2. In contrast, the Ag foil electrodes completely lost their CO_2RR activity under the same testing conditions, resulting in FE_{CO} and j_{CO} values close to 0 across different potentials (Figure 4e). The missing faradaic efficiency in both Figure 4b and e is ascribed to the SO_2 reduction reaction. SO_2 reduction mainly produce H_2S and elemental S (Table S4), however, due to the detection limitation, we do not detect significant amounts of S^{2-} and elemental S. Our ion chromatography (IC) results of post-reaction electrolytes only confirmed the presence of sulfite (SO_3^{2-}) and sulfate (SO_4^{2-}) in the catholyte, while only SO_4^{2-} was detected in the anolyte (Figure S10). Notably, formate was identified in both the cathodic and anodic compartments for the Ag electrode (Figure S10b), indicating that formate is a minor CO_2RR product on Ag surfaces. Since an anion exchange membrane is used, both formate and sulfite can readily diffuse into the anolyte, where they are subsequently oxidized to CO_2 and sulfate, respectively. Due to the dissolution of SO_2 in the electrolyte, the detection limitation of various reduction products, and the crossover of sulfur-containing anions to the anolyte, it proved challenging to accurately quantify the faradaic efficiency for sulfur-containing species.

The CO_2RR performance of ANBC electrodes was further evaluated under the influence of 1000 and 100 ppm of SO_2 at three different potentials: −0.7, −1.0, and −1.3 V vs RHE. The variations in FE_{CO} and j_{CO} under these conditions were compared to those observed in a pure CO_2 environment. As shown in Figure 4c, the presence of SO_2 impurities only significantly hampers the CO_2RR performance at high concentrations (10,000 ppm) or at less negative potentials (1000 ppm of SO_2 at −0.7 V vs RHE). At more negative potentials (−1.0 and −1.3 V vs RHE), the impact of 1000 and 100 ppm of SO_2 on FE_{CO} and j_{CO} is minimal, with performances comparable to that of pure CO_2. Interestingly, the FE_{H2} of ANBC electrodes in the presence of 100 ppm of SO_2 at −1.0 and −1.3 V vs RHE, as well as in the presence of 1000 ppm of SO_2 at −1.3 V vs RHE, is even slightly lower than that observed with pure CO_2. This reduction in FE_{H2} is likely due to competition between the hydrogen evolution reaction (HER) and the SO_2 reduction reaction.

In comparison, Ag foil electrodes exhibit greater sensitivity to SO_2 impurities (Figure 4f). Even at a low concentration of 100 ppm of SO_2 in the CO_2 feed, the FE_{CO} decreases by approximately 5% after 1 h at −1.0 V vs RHE. However, applying more negative potentials mitigates the adverse effects of SO_2. At −1.3 V vs RHE, the FE_{CO} and j_{CO} of Ag foil in the presence of 1000 and 100 ppm of SO_2 closely match those obtained with pure CO_2. These observed experimental results are comparable with the previous studies. For instance, Luc et al. reported that 100 ppm of SO_2 has a minimal impact on the CO_2RR performance of Ag catalysts during a 30 min test at a constant current density of 100 mA/cm^2, where the potential is around −1.8 V vs Ag/AgCl, corresponding to approximately −1.2 V vs RHE in 1 M $KHCO_3$ (pH = 7.8).[14] Similarly, Van Daele et al. demonstrated that 200 ppm of SO_2 did not significantly affect the product selectivity of Ag catalysts over a 20-h test at 100 mA/cm^2, where the potential is approximately −2.2 V vs Ag/AgCl, equal to −1.6 V vs RHE (0.5 M $KHCO_3$, pH = 7.4).[41] Although previous studies have shown that low concentrations of SO_2 impurities (e.g., 100−200 ppm) have negligible impacts on the CO_2RR performance of Ag catalysts under constant current conditions (particularly at potentials more negative than −1.2 V vs RHE), these investigations did not explore potential-dependent effects. Our findings highlight that the poisoning effect of SO_2 is strongly influenced by the applied potential, with elevated SO_2 concentrations and less negative potentials causing more severe performance degradation. This underscores the importance of optimizing reaction conditions to mitigate the adverse effects of SO_2 in practical CO_2 electroreduction systems.

In summary, the ANBC electrodes demonstrate superior tolerance to SO_2 impurities compared to Ag foil electrodes. Additionally, the CO_2RR performance of both ANBC and Ag foil electrodes is significantly influenced by the SO_2 concentration and the applied potential, with lower SO_2 concentrations and more negative potentials effectively mitigating the detrimental impact of SO_2 on CO_2 reduction.

Stability and Robustness of ANBC and Silver Electrodes during CO_2RR in the Presence of SO_2

To further assess the stability of the ANBC electrodes under CO_2 reduction conditions, 8-h electrolysis tests were conducted

https://doi.org/10.1021/jacs.5c11790
J. Am. Chem. Soc. XXXX, XXX, XXX−XXX

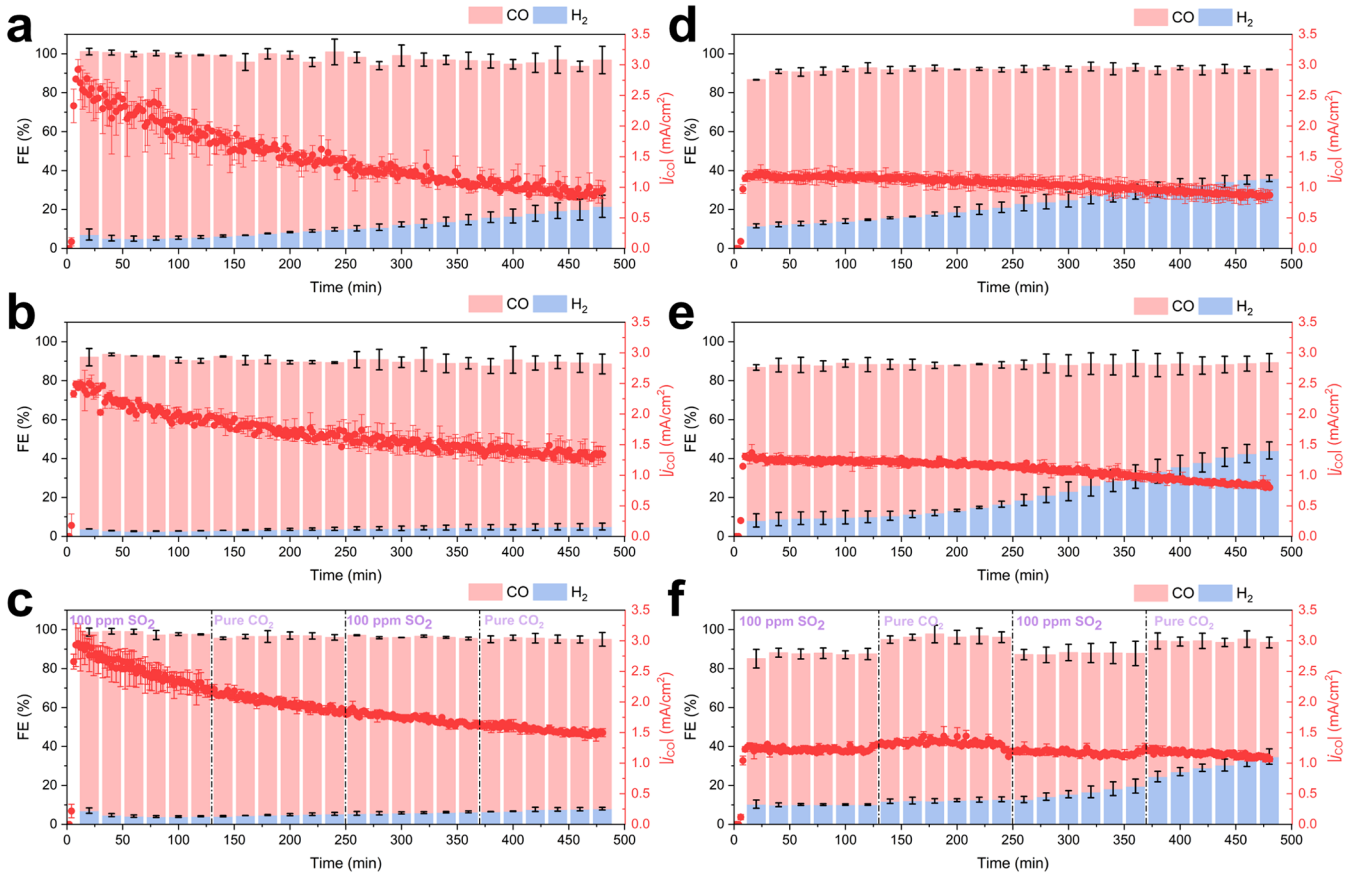

Figure 5. Longer-term CO_2 reduction performance tests. Faradaic efficiencies and j_{CO} during 8-h stability tests for (a) ANBC and (d) Ag foil electrodes at −1.0 V vs RHE in a CO_2-saturated 0.1 M $KHCO_3$ electrolyte. Faradaic efficiencies and j_{CO} during 8-h stability tests for (b) ANBC and (e) Ag foil electrodes at −1.0 V vs RHE in a CO_2 + 100 ppm of SO_2 gas mixture saturated 0.1 M $KHCO_3$ electrolyte. Faradaic efficiencies and j_{CO} of CO_2 + 100 ppm of SO_2 and pure CO_2 electrolysis over (c) ANBC and (f) electrode at −1.0 V vs RHE in 0.1 M $KHCO_3$ electrolyte over 8 h, the gas feed is modulated every 2 h.

using pure CO_2 and CO_2 containing 100 ppm of SO_2 at −1.0 V vs RHE. During continuous electrolysis with pure CO_2, the FE_{CO} of ANBC shows a decrease from 94% to 75% after 8 h (Figure 5a). Interestingly, in the presence of 100 ppm of SO_2, the ANBC electrode maintained a stable FE_{CO} above 85% and a low FE_{H2} (below 5%) over the same period (Figure 5b). These findings are consistent with the 1-h electrolysis results, indicating that the low concentration of SO_2 does not significantly impair the CO_2RR performance of the ANBC electrode. Moreover, the presence of SO_2 even appears to suppress hydrogen evolution due to competition of both reactions.

Notably, the j_{CO} gradually decreased from approximately −2.5 mA/cm^2 to −1.3 mA/cm^2 over the 8-h test. This decrease is unlikely to result from catalyst deactivation, as the product selectivity remained consistent, with FE_{CO} sustaining values above 85% throughout the experiment. It is also important to note that similar trends in j_{CO} were observed in all stability and robustness tests with ANBC electrodes, regardless of the feedstock composition (Figure 5a−c). This decrease in j_{CO} might attributed to the gradual detachment of drop-casted ANBC particles from the electrode surface, likely caused by continuous gas stream perturbations and binder degradation. Similar declines in current density for CO_2RR with drop-casted catalysts have been reported in previous studies, such as in the 12-h stability test by Hu et al.[42]

To clarify whether the decay in j_{CO} originates from sulfur-induced deactivation or physical detachment of the catalyst, a series of binder-controlled experiments were conducted. ANBC electrodes prepared without an ionomer binder exhibit a substantially faster decline in j_{CO} compared with Nafion-containing electrodes under otherwise identical conditions (100 ppm of SO_2, −1.0 V vs RHE, 4-h tests), while the corresponding FE_{CO} remains nearly constant in both cases (Figure S11a, b). The decoupling between current density decay and product selectivity suggests a gradual loss of electrochemically active surface area rather than irreversible sulfur poisoning, which would be expected to reduce CO selectivity.

To further distinguish adhesion effects from potential porosity-related contributions, a sulfur-free ionomer (FAA) was employed as an alternative binder. The ANBC−FAA electrodes show a j_{CO} decay rate comparable to that of Nafion-containing electrodes and significantly slower than that of ionomer-free ANBC, while maintaining stable FE_{CO} throughout electrolysis (Figure S11c). This trend indicates that the presence of an ionomer primarily enhances the mechanical integrity of the catalyst layer, rather than altering the intrinsic reaction selectivity or SO_2 tolerance of ANBC.

Additional qualitative evidence for catalyst detachment was obtained from postelectrolysis catholyte analysis. After several days of sedimentation, a thin black deposit was observed only in the catholyte collected from ionomer-free ANBC electrodes, whereas no visible sediment formed in the catholytes from

https://doi.org/10.1021/jacs.5c11790
J. Am. Chem. Soc. XXXX, XXX, XXX−XXX

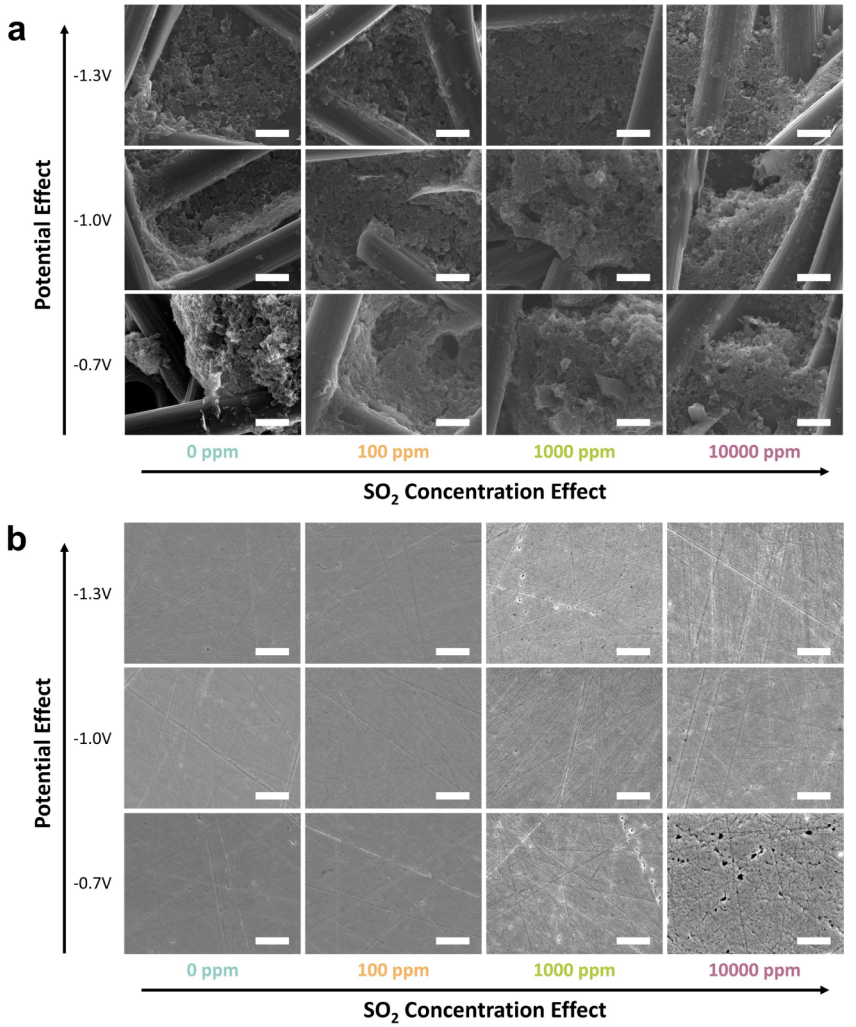

Figure 6. Surface characterization of ANBC and silver electrodes after electrolysis. SEM images of (a) ANBC (scale bar: 5 μm) and (b) Ag foil (scale bar: 2.5 μm) electrodes after 1 h electrolysis in the presence of different concentration of SO_2 impurities and different potentials.

Nafion- or FAA-containing electrodes (Figure S12). Collectively, these observations support that the observed j_{CO} decay mainly arises from partial physical detachment of drop-cast ANBC particles under gas-evolving conditions, while the intrinsic resistance of ANBC toward SO_2-induced chemical poisoning remains preserved.

In contrast, the FE_{CO} of the Ag foil electrode decreased steadily from 78% to 56% over 8 h of continuous electrolysis with pure CO_2 (Figure 5d). When 100 ppm of SO_2 was introduced into the CO_2 feed, a more pronounced drop in FE_{CO} was observed, declining from 79% to 45% (Figure 5e). This significant reduction over the extended electrolysis period is attributed to the accumulation of sulfur-containing impurities on the Ag foil surface. However, the j_{CO} for the Ag foil remained comparatively stable, likely due to the structural integrity of the Ag foil, unlike the ANBC electrode where particle detachment is a concern.

It is important to note that the decrease in FE_{CO} in this study is different from the previous study from Van Daele et al., who observed a stable FE_{CO} during a 20-h CO_2RR stability test with 200 ppm of SO_2 under a fixed current density.[41] This discrepancy can be explained by two factors: the more negative potential used in their study (approximately −2.2 V vs Ag/AgCl) likely mitigated the SO_2 poisoning effect, and the differences in cell configurations. Specifically, their setup employed a 3-compartment flow cell with continuous catholyte renewal, allowing for efficient removal of dissolved SO_2. As a result, the extent of SO_2 interaction with the Ag gas diffusion electrode (GDE) was minimized.

In contrast, our experiments were conducted using a 2-compartment H-cell, where the SO_2, due to its higher solubility compared to CO_2, accumulates in the limited volume of catholyte (1.8 mL of 0.1 M $KHCO_3$) over time. This accumulation leads to prolonged exposure of the Ag electrode to a SO_2-saturated electrolyte, which intensifies the negative impact of SO_2 on CO_2RR performance.

Overall, the differences in results between our study and that of Van Daele et al. highlight the crucial role of cell configuration and operating conditions in determining catalyst performance. Flow cells, with their ability to handle higher current densities, provide valuable insights for scaling up CO_2 electrolysis for industrial applications. In contrast, H-cells are well-suited for fundamental studies, offering a controlled environment to investigate the intrinsic behavior of catalysts in the presences of varying concentrations of SO_2 impurities. Understanding these differences is essential for designing experimental setups that align with the desired research objectives.

https://doi.org/10.1021/jacs.5c11790
J. Am. Chem. Soc. XXXX, XXX, XXX−XXX

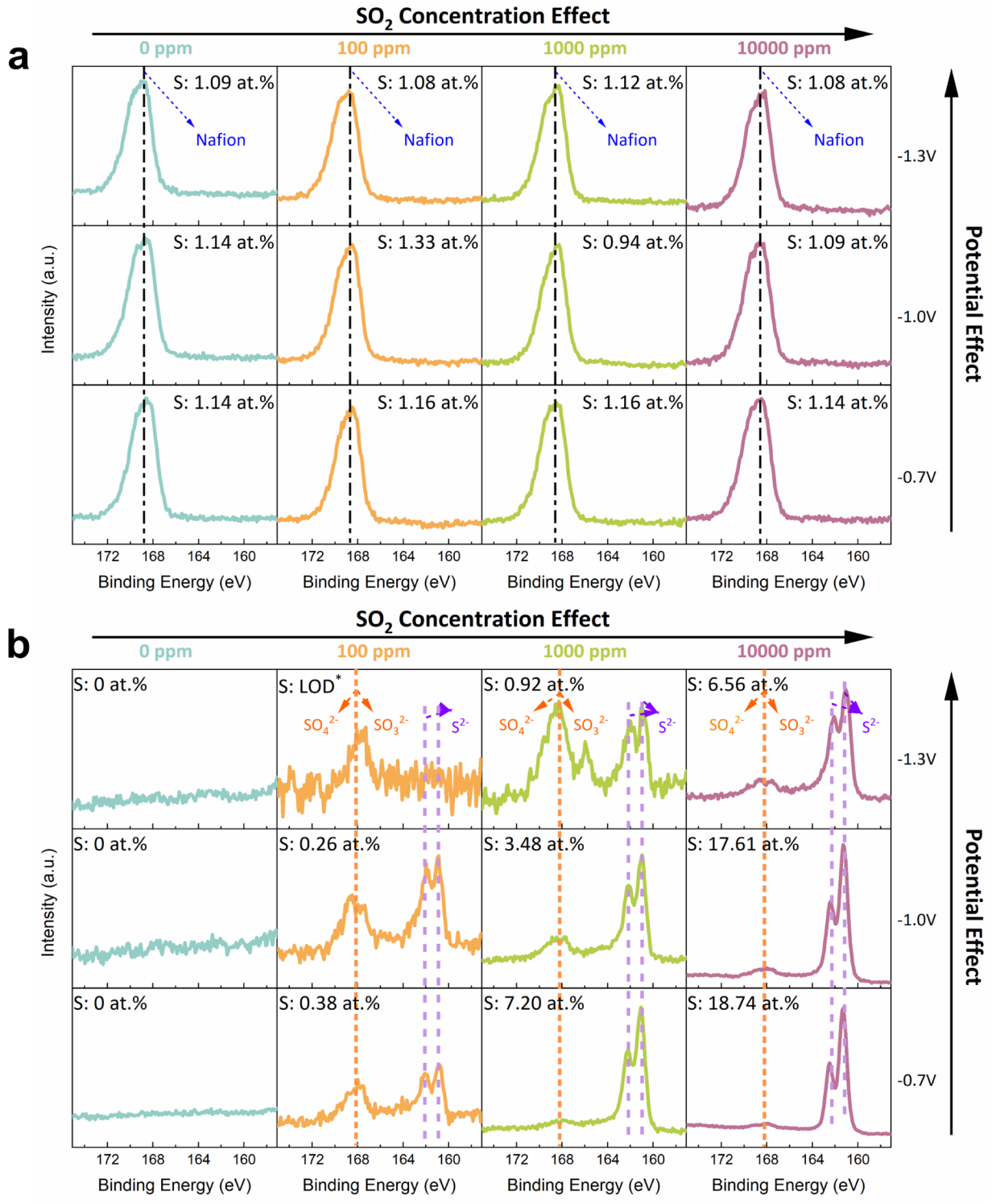

Figure 7. Characterization of the chemical composition of ANBC and silver electrodes after electrolysis. S 2p XPS spectrum of (a) ANBC and (b) Ag foil electrodes after 1 h electrolysis in the presence of different concentration of SO_2 impurities and different potentials. (*LOD = the limit of detection).

To assess the robustness of the ANBC electrode under fluctuating SO_2 concentrations typical of real flue gas, we alternated the feed gas between pure CO_2 and CO_2 containing 100 ppm of SO_2 every 2 h at −1.0 V vs RHE. As illustrated in Figure 5c, the ANBC electrodes demonstrate high tolerance to changes in the gas composition, with variations in the overall Faradaic efficiency and FE_{CO} of less than 1.5%. In contrast, the Ag foil electrode exhibits greater sensitivity to feed gas alterations (Figure 5f). During the initial 2 h with 100 ppm of SO_2 in the CO_2 feed, the FE_{CO} was approximately 75%, rising to 81% when switched to pure CO_2. However, the FE_{CO} dropped again to 72% upon reintroduction of SO_2, with significant variations in j_{CO} as well. Over time, a significant decline in the FE_{CO} can be clearly observed even during pure CO_2 feeding,

https://doi.org/10.1021/jacs.5c11790
J. Am. Chem. Soc. XXXX, XXX, XXX−XXX

likely due to cumulative sulfur contamination on the Ag surface. This robustness study highlights the significance of catalyst stability under fluctuating SO_2 concentrations, which closely mimics real-world variations in flue gas composition. The ANBC electrode's stable performance under alternating gas compositions indicates its strong tolerance to fluctuations, which is essential for maintaining consistent CO_2RR activity in dynamic industrial settings. In contrast, the Ag foil electrode shows marked sensitivity to SO_2 concentration changes, resulting in significant performance degradation. This demonstrates that ANBC is a more resilient catalyst, capable of operating effectively even in challenging and variable environments, making it a promising candidate for large-scale CO_2 electrolysis applications.

Characterization of Surface Morphology and Chemical Composition after Electrolysis

To elucidate the impact of SO_2 impurities on the surface properties of the ANBC and Ag electrodes, we conducted detailed characterizations using scanning electron microscopy (SEM) and X-ray photoelectron spectroscopy (XPS) to investigate changes in their surface morphology and chemical composition. The SEM images of the used ANBC electrodes, collected after 1 h of electrolysis under various SO_2 concentrations, did not reveal noticeable morphological alterations compared to the pristine sample (Figures 6a and S13a). Similarly, XPS analyses of pre- and postreaction ANBC electrodes showed an intensive peak at 168.7 eV, with a consistent sulfur content of approximately 1.1 at. %, corresponding to sulfur-containing groups in the Nafion binder (Figures 7a and S13b).[43] Even after 8 h of continuous electrolysis with 100 ppm of SO_2 at −1.0 V vs RHE, both the surface morphology and sulfur content (1.07 at. %) of the ANBC electrodes remained relatively unchanged (Figure S14). Additionally, XPS analysis of ionomer-free ANBC electrodes after 4 h of electrolysis reveals only an extremely weak S 2p feature centered at ∼168−169 eV, with no other identifiable sulfur-related peaks observed. This signal is most likely associated with adsorbed sulfite (SO_3^{2-}) or sulfate (SO_4^{2-}) species from the electrolyte. Consistently, ANBC electrodes prepared with a sulfur-free ionomer binder (FAA) also exhibit no measurable accumulation of reduced sulfur species after reaction (Figure S11d, e). These results collectively confirm that the absence of sulfur accumulation is intrinsic to the ANBC material and not masked by the presence of sulfur-containing binders. The SEM and XPS analyses indicate that the ANBC electrodes exhibit strong structural stability and resistance to sulfur incorporation in the presence of SO_2 impurities. This stability highlights that the observed faradaic efficiency losses of ANBC in the presence of SO_2 impurities are primarily due to competitive SO_2 reduction rather than catalyst deactivation or surface reconfiguration.

In contrast, postreaction SEM images of Ag foil electrodes exposed to 10,000 ppm of SO_2 revealed significant surface pitting, indicative of corrosion (Figure 6b). Reducing the SO_2 concentration or applying more negative potentials are helpful to mitigate the surface morphology changes (Figure 6b). The surface morphology of Ag electrodes after 1-h electrolysis in 100 ppm of SO_2 or pure CO_2 showed minimal changes compared to the fresh Ag foil (Figure S15a). XPS results further confirmed the formation of sulfur-containing species on the Ag surface (Figures S15b and 7b), with peaks at 161.1 and 162.2 eV corresponding to silver sulfide (Ag_2S) formation.[44] Additionally, trace amounts of sulfite (SO_3^{2-}) and sulfate (SO_4^{2-}) were also detected, likely originating from the electrolyte.[14] Notably, higher SO_2 concentrations favored the formation of Ag_2S, whereas more negative potentials significantly reduced the extent of sulfur incorporation. The variation in sulfur content on the Ag surface reflects a dynamic equilibrium between the formation and reduction of Ag_2S during CO_2RR in the presence of SO_2 impurities. Under cathodic conditions, adsorbed sulfur-containing intermediates react with metallic Ag to form Ag_2S, while increasingly negative potentials simultaneously promote the electrochemical reduction of Ag_2S back to Ag^0. The quantified sulfur content obtained by XPS therefore represents a balance between these competing processes. At more negative potentials, the reduction kinetics become faster, leading to a lower detectable sulfur content; however, the rate of Ag_2S formation remains dominant, resulting in gradual sulfur accumulation and the eventual deactivation of the Ag catalyst. It is also important to note that the precise formation mechanism of Ag_2S remains unclear, and future work should focus on in situ measurements to further elucidate this process.

After 8 h of electrolysis with 100 ppm of SO_2 at −1.0 V vs RHE, the surface morphology of the Ag foil electrode was similar to a fresh electrode (Figure S16a). However, the sulfur content increased markedly from 0.26 at. % (after 1 h) to 4.25 at. % (after 8 h), indicating substantial accumulation of sulfur-containing impurities on the Ag surface (Figure S16b). The SEM and XPS results for the Ag foil electrode reveal that SO_2 impurities lead to noticeable surface degradation, particularly at high concentrations or less negative potentials. SEM images show pitting and corrosion effects, while XPS analysis confirms the formation and accumulation of sulfur-containing species, such as Ag_2S, sulfite, and sulfate, on the Ag surface. This accumulation becomes more pronounced over extended electrolysis durations, significantly impacting CO_2RR performance. Thus, the decline in faradaic efficiency on Ag electrodes is attributed not only to competitive SO_2 reduction but also to the progressive formation of Ag_2S, which hinders catalytic activity.

To further elucidate the role of SO_2 in the deactivation mechanism, a series of control experiments were conducted. First, CO_2 containing 100 ppm of SO_2 was introduced into the H-cell reactor under open-circuit conditions for 1 h. XPS analysis revealed no detectable S^{2-} signals on either the ANBC or Ag foil electrodes (Figure S17), indicating that the formation of Ag_2S occurs exclusively during electrochemical operation rather than through spontaneous chemical adsorption.

To exclude the possibility that dissolved sulfur species such as SO_3^{2-} or SO_4^{2-} are responsible for catalyst deactivation, additional control experiments were performed by introducing 25 mM K_2SO_3 and 25 mM K_2SO_4 into the electrolyte, while maintaining pure CO_2 as the feed gas. After 4 h of electrolysis, both the ANBC and Ag foil electrodes exhibited negligible changes in FE_{CO} (Figure S18), confirming that SO_3^{2-} and SO_4^{2-} species do not contribute significantly to the observed deactivation. These findings collectively show that the primary degradation pathway on Ag catalysts is associated with the electrochemical formation and accumulation of Ag_2S, whereas ANBC exhibits remarkable resilience against SO_2-induced poisoning due to its chemically robust carbon−nitrogen framework and weak interaction with sulfur-containing intermediates.

These results demonstrate a stark contrast between the behavior of ANBC and Ag foil electrodes in the presence of SO_2 impurities. While the ANBC electrode remains structurally

https://doi.org/10.1021/jacs.5c11790
J. Am. Chem. Soc. XXXX, XXX, XXX−XXX

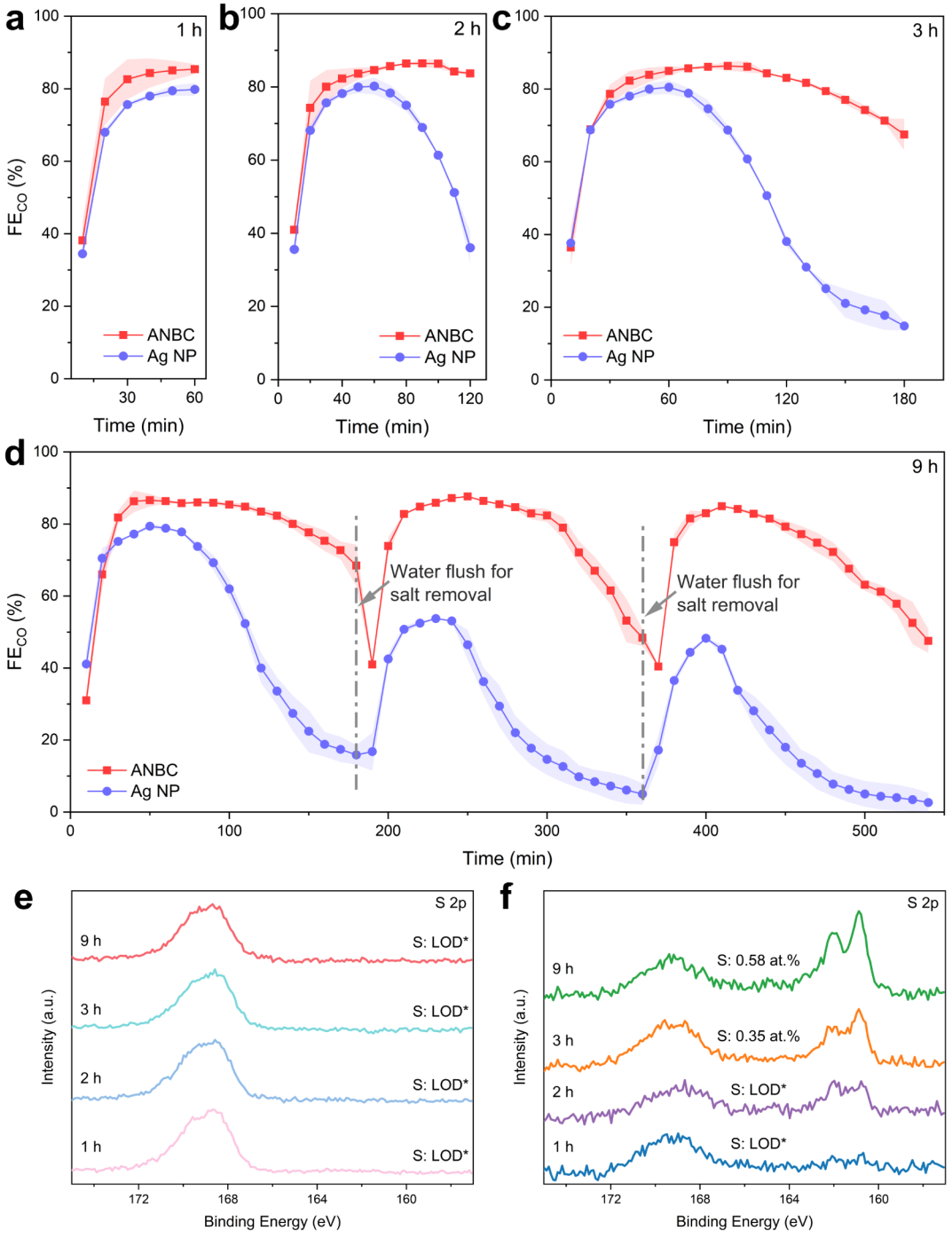

Figure 8. High current density CO_2 electrolysis tests of ANBC and Ag NP catalysts conducted in an MEA reactor in the presence of 100 ppm of SO_2. FE_{CO} of ANBC and Ag NP catalysts with reaction duration of (a) 1 h, (b) 2 h, (c) 3 h, and (d) 9 h. High-resolution S 2p XPS spectra of (e) ANBC and (f) Ag NP gas diffusion electrodes after different electrolysis durations.

intact with no significant morphological changes or sulfur incorporation, the Ag foil experiences surface pitting and extensive accumulation of sulfur-containing species, leading to severe performance degradation. The superior stability of ANBC, even at prolonged exposure and varying SO_2 concentrations, highlight its strong tolerance to sulfur impurities compared to conventional Ag catalysts.

Validation via High Current Density Operation in a Membrane Electrode Assembly Electrolyzer

To further evaluate the performance and durability of the catalysts under gas-fed and high current density conditions, we conducted CO_2 reduction tests using a membrane electrode assembly (MEA) electrolyzer (Figure S19). This setup allows for the evaluation of catalyst performance in a gas-fed configuration, more closely resembling realistic CO_2 electrolysis systems. Both the ANBC and Ag nanoparticle (Ag NP) electrodes were subjected to CO_2 electrolysis in the presence of 100 ppm of SO_2 impurities at a total current density of 100

https://doi.org/10.1021/jacs.5c11790
J. Am. Chem. Soc. XXXX, XXX, XXX−XXX

mA/cm^2, and the catalytic performance of both electrodes was evaluated for 1, 2, 3, and 9 h of operation.

As shown in Figure 8a, both catalysts exhibited stable FE_{CO} during the initial hour of operation, with ANBC achieving 87% and Ag NP maintaining 78%, indicating that short-term exposure to low SO_2 concentrations does not significantly affect CO_2RR activity. However, as electrolysis progressed, a gradual decline in FE_{CO} was observed in both systems. The ANBC electrode showed a moderate decrease to 84% after 2 h and 70% after 3 h, whereas the Ag NP electrode exhibited a much sharper decline to 32% and 15% over the same period (Figure 8b and c). This deterioration can be attributed to catalyst poisoning and/or the accumulation of carbonate salts in the cathode flow channel, which can block active sites and hinder mass transport.

To distinguish between these two deactivation pathways, intermittent rinsing of the cathode flow channel was performed every 3 h using 50 mL of deionized water to remove precipitated salts.[45] Remarkably, the ANBC electrode recovered its initial FE_{CO} value after each rinsing cycle, followed by a gradual decline upon continued operation, confirming that salt accumulation was the dominant cause of temporary performance loss. In contrast, the Ag NP electrode failed to restore its initial activity even after rinsing, suggesting irreversible deactivation, most likely due to sulfur poisoning and the formation of Ag_2S species (Figure 8d).

XPS analysis further supported these observations. For ANBC, no significant sulfur accumulation was detected even after extended electrolysis, and only weak signals associated with Nafion sulfonate groups and trace sulfite/sulfate species were observed (Figure 8e). In contrast, the Ag NP electrode displayed progressively intensified S 2p peaks at 161.1 and 162.2 eV, characteristic of Ag_2S formation, indicating severe sulfur-induced degradation during prolonged operation (Figure 8f).

We further monitored the evolution of sulfur-containing species in the anolyte of the MEA during operation using ion chromatography. The results show that in the MEA configuration with an anion exchange membrane, SO_4^{2-} is detectable in the anolyte for both ANBC and Ag NP cathodes, with SO_4^{2-} concentrations increasing with electrolysis time (Figure S20). In addition, formate ions were observed only in the anolyte of the Ag NP cathode system, with concentrations also increasing over time. These findings are consistent with the types of anionic species detected in the H-cell experiments. It should be noted that, although the detection of sulfate in the anolyte confirms the crossover of sulfur species through the membrane, establishing a complete sulfur mass balance in the current MEA configuration remains challenging. First, no liquid-phase catholyte is available for direct sampling, limiting the quantitative analysis of sulfur-containing species generated at the cathode. Second, some reduced sulfur species (e.g., S^{2-}) are unstable under near-neutral conditions and can be lost as volatile H_2S. Therefore, the IC results in this study primarily provide qualitative insight into sulfur migration rather than a strict sulfur mass balance.

These high current density experimental results are highly consistent with the observations obtained from the H-cell experiments, confirming the reliability and universality of our findings across different electrochemical configurations. Both studies demonstrate that the ANBC catalyst maintains CO_2RR activity and selectivity even in the presence of SO_2 impurities, while Ag-based catalysts suffer from rapid and irreversible deactivation due to sulfur poisoning. The agreement between the two systems strongly supports the intrinsic SO_2 tolerance and structural robustness of ANBC. Overall, this work highlights nitrogen-doped carbon catalysts as durable and cost-effective candidates for CO_2 electroreduction under sulfur-containing feed conditions, demonstrating strong resistance to SO_2-induced degradation.

CONCLUSIONS

This study demonstrates an advancement in the development of electrocatalysts for CO_2 reduction under realistic, impurity-laden conditions. Specifically, we reveal that N-doped carbon catalysts possess a remarkable tolerance to SO_2 impurities. DFT calculations indicated that N-doped carbon materials display reduced adsorption affinities for both SO_2 and *SOOH species when compared to Ag electrodes. The interaction between sulfur-based compounds and the active sites of N-doped carbon is primarily mediated by weak van der Waals forces. Additionally, the orbital overlap between SO_2 molecules and the carbon surface is less pronounced than that observed with Ag. These combined effects suggest that N-doped carbon materials exhibit greater resistance to SO_2-induced catalyst deactivation, positioning them as viable and more resilient alternatives to Ag electrodes for CO_2RR to CO in the presence of SO_2 impurities.

By conducting a series of electrochemical, structural, and surface composition analyses, we demonstrated that the ANBC electrodes exhibit significantly enhanced SO_2 tolerance and superior CO_2RR performance compared to the Ag foil electrodes. The ANBC catalyst achieved a higher faradaic efficiency toward CO than Ag foil electrode in a wide potential window and displayed stronger tolerance to SO_2 impurities. The presence of lower SO_2 concentrations (1000 and 100 ppm) caused minimal changes in CO_2RR activity, especially at more negative potentials, while only an extremely high SO_2 concentration (10,000 ppm) severely diminished CO_2RR performance due to the preferential reduction of SO_2. Notably, the ANBC catalyst maintained a stable FE_{CO} above 90% during an 8-h stability test at −1.0 V vs RHE with 100 ppm of SO_2. Overall, the ANBC electrode maintained a high CO selectivity and stability in the presence of varying concentrations of SO_2, with minimal changes in surface morphology and chemical composition observed via SEM and XPS analyses. In contrast, the Ag foil electrodes exhibited a greater sensitivity to SO_2 impurities, particularly at higher SO_2 concentrations and less negative potentials, due to the accumulation of Ag_2S and other sulfur-containing species, which progressively impaired its catalytic activity.

To further validate the practical applicability of ANBC under gas-fed conditions, we conducted high current density CO_2 electrolysis in a membrane electrode assembly reactor. The results confirmed that ANBC maintained high CO selectivity and structural integrity even at elevated current densities. In contrast, Ag nanoparticle electrodes exhibited rapid and irreversible deactivation due to Ag_2S formation and accumulation. These MEA findings are consistent with the H-cell results, reinforcing the superior SO_2 tolerance and robustness of ANBC under practical electrolysis conditions.

In conclusion, the ANBC electrodes demonstrated a clear advantage over Ag electrodes in terms of its resilience to SO_2 poisoning and long-term CO_2RR performance stability, making it a promising candidate for CO_2 electroreduction applications in SO_2-contaminated feeds. The successful validation of ANBC performance in an MEA electrolyzer demonstrates its potential scalability and applicability in advanced CO_2 electroreduction systems. Future research should focus on optimizing the ANBC catalyst to further enhance its durability and exploring its

https://doi.org/10.1021/jacs.5c11790
J. Am. Chem. Soc. XXXX, XXX, XXX−XXX

integration in large-scale flow cell systems to bridge the gap between laboratory studies and industrial applications.

■ ASSOCIATED CONTENT

Supporting Information

The Supporting Information is available free of charge at https://pubs.acs.org/doi/10.1021/jacs.5c11790.

Computational methods and experimental details; Figures for IGMH and DOS/PDOS/OPDOS analysis for SO_2/CO_2 adsorption on different active sites; additional data for material characterization (XRD, Raman, N_2 adsorption−desorption, XPS); schematic illustration of the setup; GC calibration curves; ion chromatography results of electrolytes; SEM and XPS results of ANBC and Ag foil electrodes; control experiments; and illustration of MEA reactor and supplementary tables and references (PDF)

■ AUTHOR INFORMATION

Corresponding Author

Ruud Kortlever − *Large-Scale Energy Storage, Process & Energy Department, Faculty of Mechanical Engineering, Delft University of Technology, Delft 2628 CB, The Netherlands; e-Refinery Institute, Delft University of Technology, Delft 2628 CB, The Netherlands;* orcid.org/0000-0001-9412-7480; Email: r.kortlever@tudelft.nl

Authors

Shilong Fu − *Large-Scale Energy Storage, Process & Energy Department, Faculty of Mechanical Engineering, Delft University of Technology, Delft 2628 CB, The Netherlands; e-Refinery Institute, Delft University of Technology, Delft 2628 CB, The Netherlands*

Bowen Sha − *Engineering Thermodynamics, Process & Energy Department, Faculty of Mechanical Engineering, Delft University of Technology, Delft 2628 CB, The Netherlands; e-Refinery Institute, Delft University of Technology, Delft 2628 CB, The Netherlands*

Asvin Sajeev − *Large-Scale Energy Storage, Process & Energy Department, Faculty of Mechanical Engineering, Delft University of Technology, Delft 2628 CB, The Netherlands; e-Refinery Institute, Delft University of Technology, Delft 2628 CB, The Netherlands;* orcid.org/0000-0001-6791-7292

Ming Li − *Large-Scale Energy Storage, Process & Energy Department, Faculty of Mechanical Engineering, Delft University of Technology, Delft 2628 CB, The Netherlands; Product and Process Engineering, Chemical Engineering Department, Faculty of Applied Sciences, Delft University of Technology, Delft 2628 HZ, The Netherlands; e-Refinery Institute, Delft University of Technology, Delft 2628 CB, The Netherlands*

Thijs J. H. Vlugt − *Engineering Thermodynamics, Process & Energy Department, Faculty of Mechanical Engineering, Delft University of Technology, Delft 2628 CB, The Netherlands; e-Refinery Institute, Delft University of Technology, Delft 2628 CB, The Netherlands;* orcid.org/0000-0003-3059-8712

Othonas A. Moultos − *Engineering Thermodynamics, Process & Energy Department, Faculty of Mechanical Engineering, Delft University of Technology, Delft 2628 CB, The Netherlands; e-Refinery Institute, Delft University of Technology, Delft 2628 CB, The Netherlands;* orcid.org/0000-0001-7477-9684

Wiebren de Jong − *Large-Scale Energy Storage, Process & Energy Department, Faculty of Mechanical Engineering, Delft University of Technology, Delft 2628 CB, The Netherlands; e-Refinery Institute, Delft University of Technology, Delft 2628 CB, The Netherlands*

Complete contact information is available at: https://pubs.acs.org/10.1021/jacs.5c11790

Notes

The authors declare no competing financial interest.

■ ACKNOWLEDGMENTS

S.F. and M.L. acknowledge the PhD scholarship awarded by China Scholarship Council (CSC). A.S., W.d.J., and R.K. would like to acknowledge funding from the "Reactor, Process and System Design" project of the E2CB consortium, which is financed by NWO via the Perspective program and affiliated industrial partners under the project number P17-08. The authors thank Michel van den Brink for his help in performing the experiments, and Min Li for assistance with XPS measurements and insightful discussions. The authors acknowledge the use of computational resources of the DelftBlue supercomputer, provided by the Delft High Performance Computing Centre (https://www.tudelft.nl/dhpc).

■ REFERENCES

(1) Kortlever, R.; Shen, J.; Schouten, K. J. P.; Calle-Vallejo, F.; Koper, M. T. M. Catalysts and Reaction Pathways for the Electrochemical Reduction of Carbon Dioxide. *J. Phys. Chem. Lett.* **2015**, *6* (20), 4073−4082.

(2) Lawrence, K. R.; Kumar, A. S.; Asperti, S.; van den Berg, D.; Girichandran, N.; Kortlever, R. Advances in Electrochemical Carbon Dioxide Reduction Toward Multi-carbon Products. In *Chemical Valorisation of Carbon Dioxide*; Royal Society of Chemistry: Cambridge, UK, 2022; pp. 388−412.

(3) Birdja, Y. Y.; Pérez-Gallent, E.; Figueiredo, M. C.; Göttle, A. J.; Calle-Vallejo, F.; Koper, M. T. M. Advances and Challenges in Understanding the Electrocatalytic Conversion of Carbon Dioxide to Fuels. *Nat. Energy* **2019**, *4* (9), 732−745.

(4) De Luna, P.; Hahn, C.; Higgins, D.; Jaffer, S. A.; Jaramillo, T. F.; Sargent, E. H. What Would It Take for Renewably Powered Electrosynthesis to Displace Petrochemical Processes? *Science* **2019**, *364*, No. eaav3506.

(5) Zheng, T.; Jiang, K.; Wang, H. Recent Advances in Electrochemical CO_2-to-CO Conversion on Heterogeneous Catalysts. *Adv. Mater.* **2018**, *30* (48), 1802066.

(6) Gabardo, C. M.; Seifitokaldani, A.; Edwards, J. P.; Dinh, C.-T.; Burdyny, T.; Kibria, M. G.; O'Brien, C. P.; Sargent, E. H.; Sinton, D. Combined High Alkalinity and Pressurization Enable Efficient CO_2 Electroreduction to CO. *Energy Environ. Sci.* **2018**, *11* (9), 2531−2539.

(7) Möller, T.; Ju, W.; Bagger, A.; Wang, X.; Luo, F.; Ngo Thanh, T.; Varela, A. S.; Rossmeisl, J.; Strasser, P. Efficient CO_2 to CO Electrolysis on Solid Ni−N−C Catalysts at Industrial Current Densities. *Energy Environ. Sci.* **2019**, *12* (2), 640−647.

(8) Zheng, T.; Jiang, K.; Ta, N.; Hu, Y.; Zeng, J.; Liu, J.; Wang, H. Large-Scale and Highly Selective CO_2 Electrocatalytic Reduction on Nickel Single-Atom Catalyst. *Joule* **2019**, *3* (1), 265−278.

(9) Abdinejad, M.; Irtem, E.; Farzi, A.; Sassenburg, M.; Subramanian, S.; Iglesias van Montfort, H.-P.; Ripepi, D.; Li, M.; Middelkoop, J.; Seifitokaldani, A.; et al. CO_2 Electrolysis via Surface-Engineering Electrografted Pyridines on Silver Catalysts. *ACS Catal.* **2022**, *12* (13), 7862−7876.

(10) Wang, H.; Liu, Y.; Laaksonen, A.; Krook-Riekkola, A.; Yang, Z.; Lu, X.; Ji, X. Carbon Recycling−An Immense Resource and Key to a Smart Climate Engineering: A Survey of Technologies, Cost and Impurity Impact. *Renew. Sustain. Energy Rev.* **2020**, *131*, 110010.

(11) Legrand, U.; Apfel, U.-P.; Boffito, D. C.; Tavares, J. R. The Effect of Flue Gas Contaminants on the CO_2 electroreduction to Formic Acid. *J. CO2 Util.* **2020**, *42*, 101315.
(12) Grim, R. G.; Huang, Z.; Guarnieri, M. T.; Ferrell, J. R.; Tao, L.; Schaidle, J. A. Transforming the Carbon Economy: Challenges and Opportunities in the Convergence of Low-Cost Electricity and Reductive CO_2 Utilization. *Energy Environ. Sci.* **2020**, *13* (2), 472−494.
(13) Chu, S.; Rashid, R. T.; Pan, Y.; Wang, X.; Zhang, H.; Xiao, R. The Impact of Flue Gas Impurities and Concentrations on the Photo-electrochemical CO_2 Reduction. *J. CO2 Util.* **2022**, *60*, 101993.
(14) Luc, W.; Ko, B. H.; Kattel, S.; Li, S.; Su, D.; Chen, J. G.; Jiao, F. SO_2-Induced Selectivity Change in CO_2 Electroreduction. *J. Am. Chem. Soc.* **2019**, *141* (25), 9902−9909.
(15) Choi, B. U.; Tan, Y. C.; Song, H.; Lee, K. B.; Oh, J. System Design Considerations for Enhancing Electroproduction of Formate from Simulated Flue Gas. *ACS Sustain. Chem. Eng.* **2021**, *9* (5), 2348−2357.
(16) Zhai, Y.; Chiachiarelli, L.; Sridhar, N. Effect of Gaseous Impurities on the Electrochemical Reduction of CO_2 on Copper Electrodes. *ECS Trans.* **2009**, *19* (14), 1−13.
(17) Ko, B. H.; Hasa, B.; Shin, H.; Jeng, E.; Overa, S.; Chen, W.; Jiao, F. The Impact of Nitrogen Oxides on Electrochemical Carbon Dioxide Reduction. *Nat. Commun.* **2020**, *11*, 5856.
(18) Van Daele, S.; Hintjens, L.; Van Den Hoek, J.; Neukermans, S.; Daems, N.; Hereijgers, J.; Breugelmans, T. Influence of the Target Product on the Electrochemical Reduction of Diluted CO_2 in a Continuous Flow Cell. *J. CO2 Util.* **2022**, *65*, 102210.
(19) House, K. Z.; Baclig, A. C.; Ranjan, M.; Van Nierop, E. A.; Wilcox, J.; Herzog, H. J. Economic and Energetic Analysis of Capturing CO_2 from Ambient Air. *Proc. Natl. Acad. Sci. U. S. A.* **2011**, *108* (51), 20428−20433.
(20) Raksajati, A.; Ho, M. T.; Wiley, D. E. Techno-Economic Evaluation of CO_2 Capture from Flue Gases Using Encapsulated Solvent. *Ind. Eng. Chem. Res.* **2017**, *56* (6), 1604−1620.
(21) Hu, C.; Dai, L. Doping of Carbon Materials for Metal-Free Electrocatalysis. *Adv. Mater.* **2019**, *31* (7), 1804672.
(22) Vasileff, A.; Zheng, Y.; Qiao, S. Z. Carbon Solving Carbon's Problems: Recent Progress of Nanostructured Carbon-Based Catalysts for the Electrochemical Reduction of CO_2. *Adv. Energy Mater.* **2017**, *7* (21), 1700759.
(23) Adegoke, K. A.; Maxakato, N. W. Electrochemical CO_2 Conversion to Fuels on Metal-Free N-Doped Carbon-Based Materials: Functionalities, Mechanistic, and Technoeconomic Aspects. *Mater. Today Chem.* **2022**, *24*, 100838.
(24) Fu, S.; Li, M.; Asperti, S.; De Jong, W.; Kortlever, R. Unravelling the Effect of Activators Used in the Synthesis of Biomass-Derived Carbon Electrocatalysts on the Electrocatalytic Performance for CO_2 Reduction. *ChemSusChem* **2023**, *16* (9), No. e202202188.
(25) Fu, S.; Li, M.; de Jong, W.; Kortlever, R. Tuning the Properties of N-Doped Biochar for Selective CO_2 Electroreduction to CO. *ACS Catal.* **2023**, *13*, 10309−10323.
(26) Gerber, I. C.; Serp, P. A Theory/Experience Description of Support Effects in Carbon-Supported Catalysts. *Chem. Rev.* **2020**, *120* (2), 1250−1349.
(27) Lu, T.; Chen, Q. Independent Gradient Model Based on Hirshfeld Partition: A New Method for Visual Study of Interactions in Chemical Systems. *J. Comput. Chem.* **2022**, *43* (8), 539−555.
(28) Lu, T.; Chen, F. Multiwfn: A Multifunctional Wavefunction Analyzer. *J. Comput. Chem.* **2012**, *33* (5), 580−592.
(29) Lu, T. A Comprehensive Electron Wavefunction Analysis Toolbox for Chemists, Multiwfn. *J. Chem. Phys.* **2024**, *161* (8), 082503.
(30) Guo, M.; Ji, M.; Cui, W. Theoretical Investigation of HER/OER/ORR Catalytic Activity of Single Atom-Decorated Graphyne by DFT and Comparative DOS Analyses. *Appl. Surf. Sci.* **2022**, *592*, 153237.
(31) Cui, Y.; Ren, C.; Wu, M.; Chen, Y.; Li, Q.; Ling, C.; Wang, J. Structure-Stability Relation of Single-Atom Catalysts under Operating Conditions of CO_2 Reduction. *J. Am. Chem. Soc.* **2024**, *146*, 29169−29176.
(32) Feng, H.; Hu, H.; Dong, H.; Xiao, Y.; Cai, Y.; Lei, B.; Liu, Y.; Zheng, M. Hierarchical Structured Carbon Derived from Bagasse Wastes: A Simple and Efficient Synthesis Route and Its Improved Electrochemical Properties for High-Performance Supercapacitors. *J. Power Sources* **2016**, *302*, 164−173.
(33) Daiyan, R.; Tan, X.; Chen, R.; Saputera, W. H.; Tahini, H. A.; Lovell, E.; Ng, Y. H.; Smith, S. C.; Dai, L.; Lu, X.; Amal, R. Electroreduction of CO_2 to CO on a Mesoporous Carbon Catalyst with Progressively Removed Nitrogen Moieties. *ACS Energy Lett.* **2018**, *3* (9), 2292−2298.
(34) Zou, K.; Deng, Y.; Chen, J.; Qian, Y.; Yang, Y.; Li, Y.; Chen, G. Hierarchically Porous Nitrogen-Doped Carbon Derived from the Activation of Agriculture Waste by Potassium Hydroxide and Urea for High-Performance Supercapacitors. *J. Power Sources* **2018**, *378*, 579−588.
(35) Li, F.; Xue, M.; Knowles, G. P.; Chen, L.; MacFarlane, D. R.; Zhang, J. Porous Nitrogen−Doped Carbon Derived from Biomass for Electrocatalytic Reduction of CO_2 to CO. *Electrochim. Acta* **2017**, *245*, 561−568.
(36) Niu, J.; Shao, R.; Liu, M.; Zan, Y.; Dou, M.; Liu, J.; Zhang, Z.; Huang, Y.; Wang, F. Porous Carbons Derived from Collagen-Enriched Biomass: Tailored Design, Synthesis, and Application in Electrochemical Energy Storage and Conversion. *Adv. Funct. Mater.* **2019**, *29* (46), 1905095.
(37) Liu, W. J.; Jiang, H.; Yu, H. Q. Emerging Applications of Biochar-Based Materials for Energy Storage and Conversion. *Energy Environ. Sci.* **2019**, *12* (6), 1751−1779.
(38) Yan, C.; Jiang, X.; Yu, J.; Ding, Z.; Ma, L.; Su, T.; Wang, Y.; Wang, C.; Huang, G.; Xu, S. Waste to Wealth: Direct Utilization of Spent Materials for Electrocatalysis and Energy Storage. *Green Chem.* **2023**, *25*, 3816−3846.
(39) Harmon, N. J.; Wang, H. Electrochemical CO_2 Reduction in the Presence of Impurities: Influences and Mitigation Strategies. *Angew. Chem., Int. Ed.* **2022**, *61* (52), No. e202213782.
(40) Fornés, J. P.; González, G. A.; Bisang, J. M. Electrochemical Conversion of Sulfur Dioxide with a Rotating Cylinder Electrode Working as Anode or Cathode. *J. Chem. Technol. Biotechnol.* **2016**, *91* (1), 219−225.
(41) Van Daele, S.; Hintjens, L.; Hoekx, S.; Bohlen, B.; Neukermans, S.; Daems, N.; Hereijgers, J.; Breugelmans, T. How Flue Gas Impurities Affect the Electrochemical Reduction of CO_2 to CO and Formate. *Appl. Catal. B Environ.* **2024**, *341*, 123345.
(42) Hu, X.-M.; Hval, H. H.; Bjerglund, E. T.; Dalgaard, K. J.; Madsen, M. R.; Pohl, M.-M.; Welter, E.; Lamagni, P.; Buhl, K. B.; Bremholm, M.; et al. Selective CO_2 Reduction to CO in Water Using Earth-Abundant Metal and Nitrogen-Doped Carbon Electrocatalysts. *ACS Catal.* **2018**, *8* (7), 6255−6264.
(43) Leverett, J.; Yuwono, J. A.; Kumar, P.; Tran-Phu, T.; Qu, J.; Cairney, J.; Wang, X.; Simonov, A. N.; Hocking, R. K.; Johannessen, B.; Dai, L.; Daiyan, R.; Amal, R. Impurity Tolerance of Unsaturated Ni-N-C Active Sites for Practical Electrochemical CO_2 Reduction. *ACS Energy Lett.* **2022**, *7* (3), 920−928.
(44) Ghafoor, S.; Ata, S.; Mahmood, N.; Arshad, S. N. Photo-sensitization of TiO_2 Nanofibers by Ag_2S with the Synergistic Effect of Excess Surface Ti^{3+} States for Enhanced Photocatalytic Activity under Simulated Sunlight. *Sci. Rep.* **2017**, *7* (1), 255.
(45) Endrődi, B.; Kecsenovity, E.; Samu, A.; Darvas, F.; Jones, R. V.; Török, V.; Danyi, A.; Janáky, C. Multilayer Electrolyzer Stack Converts Carbon Dioxide to Gas Products at High Pressure with High Efficiency. *ACS Energy Lett.* **2019**, *4* (7), 1770−1777.

https://doi.org/10.1021/jacs.5c11790
J. Am. Chem. Soc. XXXX, XXX, XXX−XXX